Journal of Neuroradiology 47 (2020) 197–202

Available online at ScienceDirect www.sciencedirect.com

Elsevier Masson France EM|consulte www.em-consulte.com

Original Article

Differentiation between glioblastoma and solitary brain metastasis using neurite orientation dispersion and density imaging

Yoshihito Kadota [a,*], Toshinori Hirai [a], Minako Azuma [a], Yohei Hattori [a], Zaw Aung Khant [a], Masaaki Hori [c], Kiyotaka Saito [b], Kiyotaka Yokogami [b], Hideo Takeshima [b]

[a] Departments of Radiology, Faculty of Medicine, University of Miyazaki, 5200 Kihara, Kiyotake, Miyazaki 8891692, Japan
[b] Departments of Neurosurgery, Faculty of Medicine, University of Miyazaki, Miyazaki, Japan
[c] Department of Radiology, School of Medicine, Juntendo University, Tokyo, Japan

INFO ARTICLE

Historique de l'article :
Disponible sur Internet le 12 November 2018

Keywords :
Glioblastoma
Brain metastasis
Diffusion-weighted imaging
NODDI

ABSTRACT

Background and purpose. – Neurite orientation dispersion and density imaging (NODDI) is a new technique that applies a three-diffusion-compartment biophysical model. We assessed the usefulness of NODDI for the differentiation of glioblastoma from solitary brain metastasis.
Methods. – NODDI data were prospectively obtained on a 3T magnetic resonance imaging (MRI) scanner from patients with previously untreated, histopathologically confirmed glioblastoma ($n = 9$) or solitary brain metastasis ($n = 6$). Using the NODDI Matlab Toolbox, we generated maps of the intra-cellular, extracellular, and isotropic volume (VIC, VEC, VISO) fraction. Apparent diffusion coefficient – and fraction anisotropy maps were created from the diffusion data. On each map we manually drew a region of interest around the peritumoral signal-change (PSC) – and the enhancing solid area of the lesion. Differences between glioblastoma and metastatic lesions were assessed and the area under the receiver operating characteristic curve (AUC) was determined.
Results. – On VEC maps the mean value of the PSC area was significantly higher for glioblastoma than metastasis ($P < 0.05$); on VISO maps it tended to be higher for metastasis than glioblastoma. There was no significant difference on the other maps. Among the 5 parameters, the VEC fraction in the PSC area showed the highest diagnostic performance. The VEC threshold value of ≥ 0.48 yielded 100% sensitivity, 83.3% specificity, and an AUC of 0.87 for differentiating between the two tumor types.
Conclusions. – NODDI compartment maps of the PSC area may help to differentiate between glioblastoma and solitary brain metastasis.

Introduction

Glioblastomas and brain metastases are the two most common brain tumors in the elderly [1]. As these tumors require different management strategies, their differentiation is important [2,3]. This may be possible on conventional magnetic resonance images (MRI) when multiple lesions are present and clinical information is available. However, a solitary metastatic brain lesion is the first manifestation of disease in approximately 30% of patients with systemic cancer [4] and in such patients, it can be difficult to differentiate the clinical entities because their imaging findings on conventional MRI scans can be similar.

Diffusion-weighted imaging (DWI) techniques such as diffusion tensor imaging (DTI) have been used to differentiate between glioblastoma and brain metastasis, however, there are conflicting results [5–13]. Some suggested that the apparent diffusion coefficient (ADC) [5–8] and fractional anisotropy (FA) [5,7,9–11] are helpful for their differentiation, while others questioned the usefulness of ADC [9–12] and FA [13].

Neurite orientation dispersion and density imaging (NODDI) is a DWI technique that poses a three-compartment biophysical model [intracellular, extracellular, and cerebrospinal fluid (CSF)] for each voxel. It is expected to reflect the microstructure of dendrites and axons and provides data on neuronal changes that are more specific than those provided by standard DTI analysis [14]. It has been reported that NODDI is useful for the evaluation of cortical dysplasia, Parkinson disease, and idiopathic normal pressure hydrocephalus [15–17]. This technique has also been applied in patients with brain tumors [18,19]. As the NODDI compartment model theoretically distinguishes three types of water diffusion behavior (i.e. intracellular, extracellular, and CSF), it might demonstrate the difference in water diffusion between tumor infiltration and vasogenic edema.

* Corresponding author.
Adresse e-mail : toshinorh@med.miyazaki-u.ac.jp (Y. Kadota).

https://doi.org/10.1016/j.neurad.2018.10.005

Table 1
Summary of patients and brain tumors.

Case	Age/sex	Pathology of tumors
1	79/F	Glioblastoma
2	79/F	Glioblastoma
3	65/M	Glioblastoma
4	69/F	Glioblastoma
5	66/F	Glioblastoma
6	63/F	Glioblastoma
7	44/F	Glioblastoma
8	66/M	Glioblastoma
9	64/M	Glioblastoma
10	67/M	Metastasis (unknown primary site, SCC)
11	46/M	Metastasis (lung, adenocarcinoma)
12	38/F	Metastasis (lung, adenocarcinoma)
13	79/F	Metastasis (lung, adenocarcinoma)
14	61/M	Metastasis (lung, adenocarcinoma)
15	43/F	Metastasis (lung, adenocarcinoma)

F: female; M: male; SCC: squamous cell carcinoma.

To the best of our knowledge, however, there are no reports on the usefulness of NODDI for the differentiation between glioblastoma and solitary brain metastasis. Therefore, we assessed its usefulness for the differentiation between these tumors.

Materials and methods

Patient selection

Our prospective study was approved by the Institutional Board of Research Associates; prior written informed consent was obtained from all patients. In the course of one year, we prospectively collected data from 42 consecutive patients who gave informed consent for their inclusion in this study and underwent MRI studies including NODDI for untreated solitary brain lesions. We included patients who underwent surgical resection after the MRI examination and whose diagnosis, made by an experienced pathologist, was glioblastoma or metastatic brain tumor. We excluded 27 patients due to:

- the lack of contrast-enhanced MRI scans;
- a diagnosis of other intra-axial brain tumors (e.g. lymphoma, oligodendroglioma, anaplastic astrocytoma, astroblastoma, typical teratoid/rhabdoid tumor);
- a diagnosis of extra-axial tumors (e.g. meningioma, schwannoma, dural metastasis);
- a diagnosis of non-tumor lesions (e.g. demyelinating lesion, subcortical hematoma), or;
- MRI scans with severe motion – or susceptibility artifacts.

Consequently, our study population was comprised of 15 consecutive patients (9 women, 6 men; age range 38–79 years; mean age 61.9 years) with glioblastoma or a solitary metastatic brain tumor. All underwent pre-operative MRI studies including NODDI and all harbored perifocal T2-hyperintense areas. Of the 15 patients, 9 (6 women, 3 men; mean age 66.1 years; age range 44–79 years) had glioblastoma; the other 6 (3 men, 3 women; mean age 55.7 years; age range 38–79 years) presented with brain metastasis (Table 1). All underwent surgical resection; the diagnosis was based on histopathologic findings. In patients with brain metastases ($n = 6$), the primary tumors were non-small-cell lung carcinomas ($n = 5$) in the other patient the primary site was unknown.

MRI

All scans were performed on a 3T MR unit (Inginia 3T CX, Philips) with a 32-channel head coil. Conventional MRI included axial T2-weighted imaging (WI) [TR/TE, 3500/80 ms, field of view (FOV) 220 × 200 mm^2, matrix size 386 × 269, section thickness 5 mm), T1-WI (TR/TE 450/10 ms, FOV 220 × 200 mm^2, matrix size 256 × 210, section thickness 5 mm), and contrast-enhanced T1-WI. NODDI data were obtained prior to contrast-enhanced study during the same examination.

NODDI data were acquired by using a multi-band echo planar imaging technique (multiband factor 2). The acquisition parameters were TR/TE 8741/83 ms, FOV 224 × 224 mm^2, matrix size 76 × 75, voxel size 3 × 3 × 3 mm^3, section gap 0 mm, and acquisition time 708 s. We used three b-values (0, 1000, 2000 s/mm^2) with 32 motion-probing gradient (MPG) directions for each b-value.

Image processing

NODDI data were fitted to the NODDI model [14] by using the NODDI Matlab Toolbox (http://www.nitrc.org/projects/noddi_toolbox). Maps of the intracellular- and isotropic volume (VIC, VISO) fraction were generated. The extracellular volume (VEC) fraction was derived from these compartment maps and calculated using an in house Matlab (The MathWorks) script. ADC and FA maps were created from the same diffusion data obtained at $b = 2000$ s/mm^2.

Image evaluation

One neuroradiologist manually drew a region of interest (ROI) with reference to T2- and postcontrast T1-WI. No fewer than 3 uniform round ROIs (approximately 40 mm^2) were carefully placed on the maximum cross-section of a contrast-enhanced tumor area that did not contain necrotic or hemorrhagic portions (Fig. 1c) [8]. On T2-WI scans, an ROI was placed on the whole PSC area at its maximum cross-section (Fig. 1d) to avoid subjective focal ROI placement. The ROIs were transferred to the VIC-, VISO-, and VEC fraction, the ADC, and the FA maps and the mean values of the ROIs were calculated using Image J software (NIH, Bethesda, MD).

Statistical analysis

The Mann–Whitney U-test was used to assess differences in the mean value of VIC, VISO, VEC, FA, and the ADC between glioblastoma and metastasis. The optimal threshold for differentiating the two tumor types was determined by using the Youden index and receiver operating characteristic (ROC) curves. To determine the diagnostic performance of certain parameters, the sensitivity, specificity and the area under the ROC curve (AUC) were calculated. We also performed pairwise comparison of the ROC curves. A statistical package, MedCalc for Windows (MedCalc Software, Mariakerke, Belgium), was used for all analyses. A P-value < 0.05 was considered significant.

Results

The patient characteristics and the mean values of the VIC-, VISO-, and VEC fraction, the ADC, and of FA are shown in Tables 2 and 2. With respect to the contrast-enhanced solid areas we detected no significant differences for any parameters (Table 2). In the PSC area (Table 3), the mean VEC fraction value was significantly higher in patients with glioblastoma than brain metastasis ($P < 0.05$) (Figs. 2 and 3). On VISO maps the mean value of the PSC area tended to be higher for metastasis than glioblastoma (Figs. 2 and 3) although there was no significant difference ($P = 0.077$). The mean value on the other maps was not significantly different.

Tables 4 and 5 show the threshold value and diagnostic performance of each parameter used for differentiating between

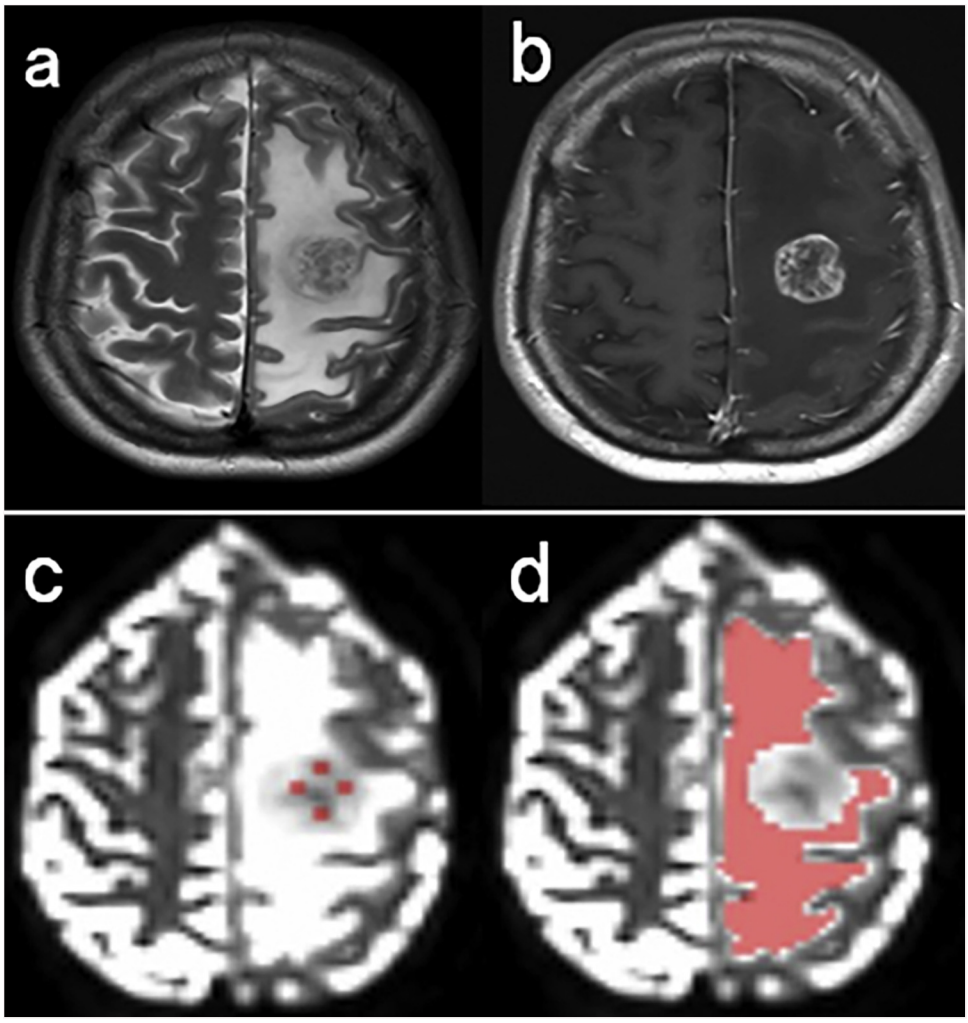

Fig. 1. An example of ROI placement in a patient with left frontal brain metastasis: a: the T2-weighted image shows a peritumoral T2-signal change area in the left cerebral white matter; b: post-contrast T1-weighted image demonstrates a heterogeneously enhancing lesion in the left frontal subcortical region; c: no fewer than 3 uniform round ROIs (approximately 40 mm^2) were placed at the maximum cross-section of the contrast-enhanced tumor area free of necrosis or hemorrhage. The ROI was then copied and pasted on VIC-, VISO-, VEC-, ADC-, and FA maps; d: an ROI encompassing the entire peritumoral signal change area was placed on its maximum cross-section on the T2-weighted image. The ROI was then copied and pasted on each map.

Table 2
Mean value of the VEC-, VIC-, and VISO fraction, the ADC, and FA in the contrast-enhanced solid area of glioblastomas and metastatic tumors.

	Glioblastoma	Metastasis	*P*-value
VEC	0.535 ± 0.088	0.370 ± 0.226	0.195
VIC	0.376 ± 0.100	0.475 ± 0.200	0.239
VISO	0.241 ± 0.099	0.264 ± 0.142	0.814
ADC	1.20 ± 0.11	1.13 ± 0.10	0.157
FA	0.145 ± 0.082	0.098 ± 0.042	0.157

Table 3
Mean value of the VEC-, VIC-, and VISO fraction, the ADC and FA in the peritumoral signal change area of glioblastomas and metastatic tumors.

	Glioblastoma	Metastasis	*P*-value
VEC	0.659 ± 0.077	0.492 ± 0.121	0.018
VIC	0.182 ± 0.059	0.200 ± 0.086	0.637
VISO	0.201 ± 0.092	0.321 ± 0.124	0.077
ADC	1.43 ± 0.17	1.57 ± 0.19	0.126
FA	0.170 ± 0.024	0.158 ± 0.065	0.099

VEC: extracellular volume fraction; VIC: intra-cellular volume fraction; VISO: isotropic volume fraction; ADC: apparent diffusion coefficient; FA: fraction anisotropy.
All values are the mean ± standard deviation.
The ADC is expressed in units of $\times 10^{-3}$ mm^2/s.

Table 4
Threshold value and diagnostic performance of each parameter in the enhancing solid tumor area for differentiating between glioblastomas and metastatic tumors.

	Threshold value	Sensitivity	Specificity	AUC	95% confidence interval
VEC	0.27	100	66.7	0.70	0.419–0.905
VIC	0.42	77.8	66.7	0.69	0.401–0.893
VISO	0.30	77.8	50.0	0.54	0.269–0.790
ADC	1.20	55.6	83.3	0.72	0.438–0.916
FA	0.10	77.8	66.7	0.72	0.438–0.916

VEC: extracellular volume fraction; VIC: intra-cellular volume fraction; VISO: isotropic volume fraction; ADC: apparent diffusion coefficient; FA: fraction anisotropy; AUC: the area under the receiver operating characteristic curve.
The ADC is expressed in units of $\times 10^{-3}$ mm^2/s.

glioblastomas and metastatic tumors. In the contrast-enhanced solid areas, none of the parameters yielded high diagnostic performance (Table 4, Fig. 4). Pairwise comparison of the ROC curves showed no significant difference between each pair of the parameters (Fig. 4). With regard to the PSC area, the VEC fraction exhibited the highest diagnostic performance among the 5 parameters for differentiating glioblastoma from brain metastasis (Table 5, Fig. 5). A VEC fraction threshold value of ≥ 0.48 yielded 100% sensitivity, 83.3% specificity, and an AUC of 0.87 for differentiating glioblas-

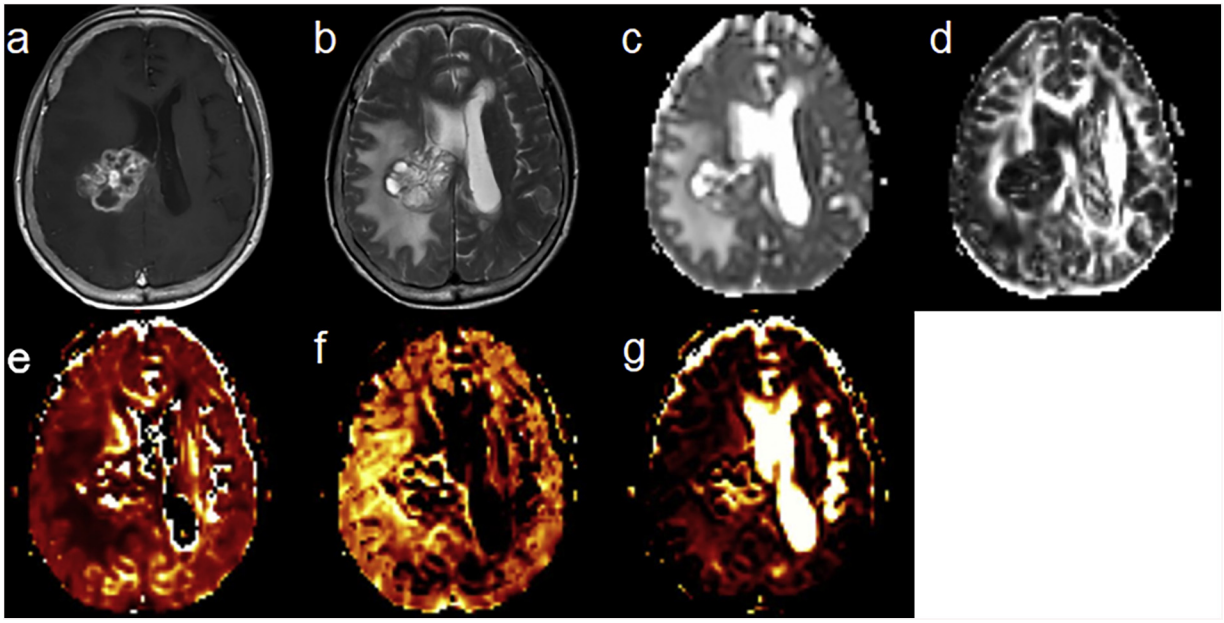

Fig. 2. Glioblastoma in the right periventricular area of a 69-year-old woman (case 4): a: contrast-enhanced T1-weighted image showing an inhomogeneously enhanced mass; b: the lesion harbors a large peritumoral hyperintense area on the T2-weighted image; c–g: compared with the contralateral normal-appearing white matter, in the peritumoral T2-hyperintense area the signal is higher on the ADC map (c), lower on the FA map (d), lower in the VIC- (e), higher in the VEC- (f), and similar on the VISO map (g). The mean value of the ADC is 1.47×10^{-3} mm^2/s. The mean value of the FA is 0.17. The mean value of the NODDI compartment map is 0.16, 0.63, and 0.21 on the VIC-, VEC-, and VISO map, respectively.

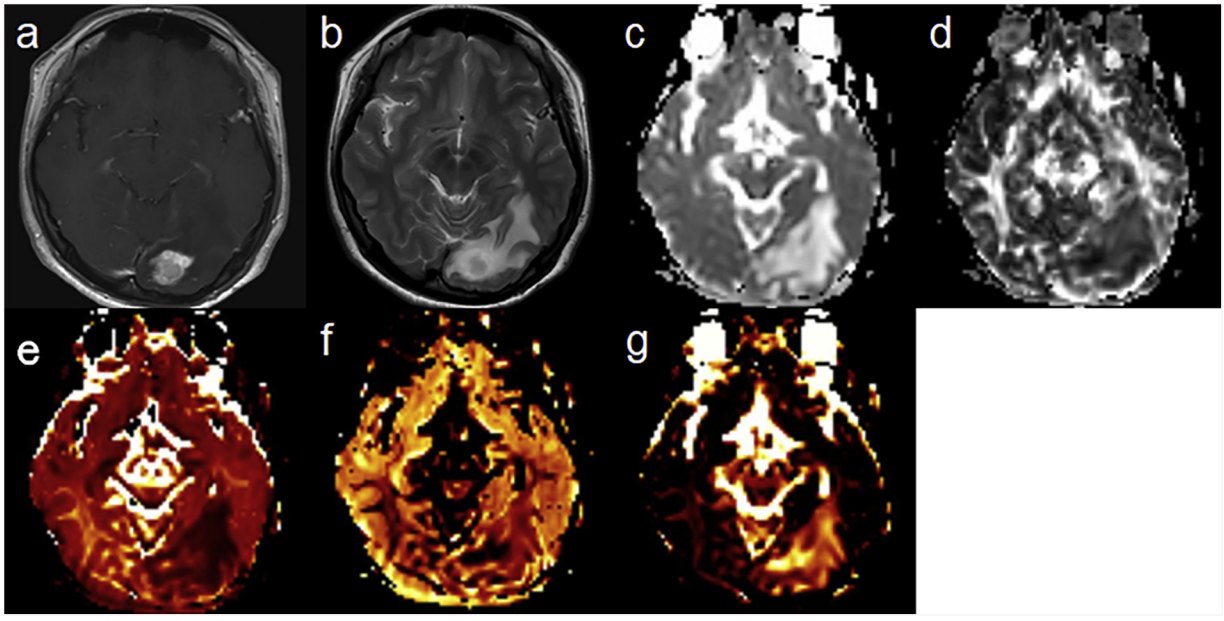

Fig. 3. Brain metastasis in left occipital lobe of a 38-year-old woman (case 12): a: contrast-enhanced T1-weighted image showing an inhomogeneously enhancing mass; b: the lesion features a moderately hyperintense peritumoral area on the T2-weighted image; c–g: compared with the contralateral normal-appearing white matter, in the peritumoral T2-hyperintense area, the signal is higher on the ADC map (c), lower on the FA map (d), lower on the VIC- (e), similar on the VEC- (f), and higher on the VISO map (g). The mean value of the ADC is 1.56×10^{-3} mm^2/s. The mean value of the FA is 0.15. The mean value of the NODDI compartment map is 0.21, 0.39, and 0.43 on the VIC, VEC, and VISO map, respectively.

toma from brain metastasis. A VISO fraction threshold of ≤ 0.24 yielded 88.9% sensitivity, 83.3% specificity, and an AUC of 0.78. In pairwise comparison of the ROC curves, there was no significant difference between each pair of the parameters (Fig. 5).

Discussion

Although ADC and FA analysis may facilitate the differentiation of glioblastoma from brain metastasis [5–11], we found that the VEC fraction in the PSC area was more useful. The NODDI compartment model theoretically distinguishes three types of water diffusion behavior (i.e. intracellular, extracellular, and CSF) according to their diffusion characteristic: Gaussian anisotropic diffusion (VEC), non-Gaussian anisotropic diffusion (VIC), and isotropic Gaussian diffusion (VISO) [14]. ADC and FA analysis does not use the compartment model. From a histopathological perspective, the PSC area in patients with metastasis reflects only vasogenic edema [20] while in patients with glioblastoma it is attributable

Table 5
Threshold value and diagnostic performance of each parameter in the peritumoral signal change area for differentiating between glioblastomas and metastatic tumors.

	Threshold value	Sensitivity	Specificity	AUC	95% confidence interval
VEC	0.48	100	83.3	0.87	0.600–0.985
VIC	0.14	44.4	93.3	0.57	0.300–0.818
VISO	0.24	88.9	83.3	0.78	0.495–0.946
ADC	1.51	77.8	83.3	0.74	0.457–0.926
FA	0.61	77.8	83.3	0.76	0.476–0.936

VEC: extracellular volume fraction; VIC: intra-cellular volume fraction; VISO: isotropic volume fraction; ADC: apparent diffusion coefficient; FA: fraction anisotropy; AUC: the area under the receiver operating characteristic curve.
The ADC is expressed in units of $\times 10^{-3}$ mm^2/s.

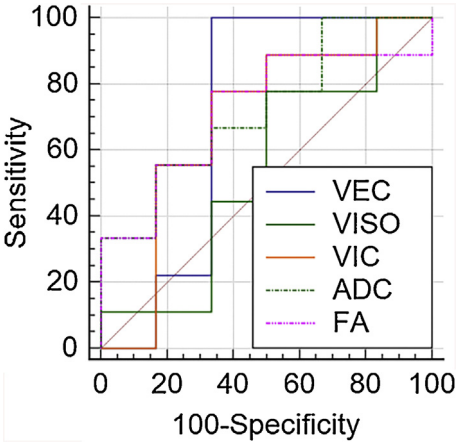

Fig. 4. ROC curves for VEC, VIC, VISO, ADC, and FA in the enhancing solid area no ROC curves show high diagnostic performance for differentiating glioblastoma from brain metastasis.

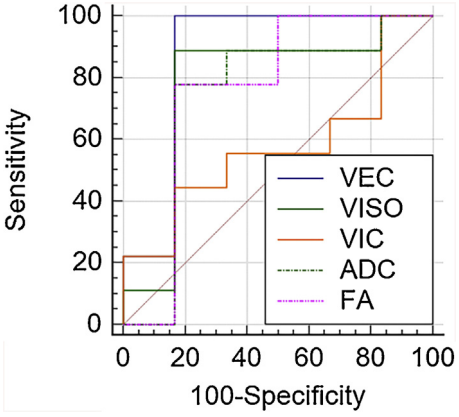

Fig. 5. ROC curves for VEC, VIC, VISO, ADC, and FA in the peritumoral signal change area.

to tumor infiltration and/or vasogenic edema [21–24]. Our findings suggest that the NODDI technique is more sensitive to these microstructural changes than either ADC or FA assessment.

Caverzasi et al. [18] applied the NODDI model on 3T MR scanners to assess various brain lesions including demyelinating disease, neoplastic processes, stroke, and toxic/metabolic disease. Although they did not systematically assess NODDI data by statistical analyses, their qualitative findings suggested that the NODDI color map is useful for identifying vasogenic edema (e.g., metastasis, lymphoma, and toxoplasmosis) characterized by a marked increase of the VISO, different from tumor-infiltrated edema, which is characterized by an associated increase in the VEC fraction (e.g. high-grade glioma). Their findings are in line with our results, but our data suggested that the VEC fraction was more useful than the VISO fraction for the differentiation of glioblastoma from brain metastasis.

Wen et al. [19] investigated the clinical feasibility of the NODDI technique at 7T for the evaluation of glioma. They evaluated normal-appearing white matter (NAWM) regions and T2 hyperintensity lesions (T2L) on FLAIR images and contrast-enhancing lesions (CEL) on post-contrast T1-WI scans of 20 patients with recurrent glioma. Within T2L and CEL, both the VISO- and the VEC fraction was significantly higher than in the NAWM region; the VIC fraction was significantly decreased. They suggested that the increased signal on VISO maps was related to vasogenic edema, the higher signal on VEC maps to invading tumor cells along fiber tracts, and the decreased signal on VIC maps to edema and loss of neurons. Our data support their suggestions.

We do not know the exact reason why the VEC- is superior to the VIC- or VISO fraction for the differentiation of glioblastoma from solitary brain metastasis. According to Zhang et al. [14], NODDI describes the diffusion MRI signal as a sum of three non-exchanging compartments:

$$S = (1 - VISO)\left\{(VIC \times Sic) + (1 - VIC) \times Sec\right\} + VISO\,Siso$$

where S is the entire normalized signal; Sic, Sec, and Siso are the normalized signals of the intracellular, extracellular, and CSF compartments, respectively; and VIC and VISO the normalized volume fractions of the intra-cellular and CSF compartments, respectively. These fractions and the signal amplitude are closely correlated. Theoretically, if one component prevails, the influence of the other components should be suppressed. Based on our results, we speculate that in the area of tumor cell infiltration, the influence of the VEC fraction was stronger than of the VIC- or VISO fraction.

Our assessment of the mean value on VIC-, VEC-, VISO-, ADC-, and FA maps of the contrast-enhanced tumor area revealed no significant difference between patients with glioblastoma or brain metastasis. Earlier studies demonstrated that the NODDI color map better visualized tumor heterogeneity by identifying different tissue components within lesions that appeared homogeneous on conventional imaging scans [18,19]. Although NODDI techniques may identify more different tissue components within tumors than conventional imaging, our results show that they may not be useful for differentiating the heterogeneity of glioblastoma and solitary brain metastasis

Our study has some limitations. First, our study population was small. Larger series are needed to assess the value of the NODDI technique for differentiating between brain tumor types. Second, we did not perform pathological evaluation of the peritumoral T2-hyperintense area. Although correlative studies between NODDI maps and pathologic findings are required to clarify the significance of the signals on NODDI maps, based on previous studies [20–24], the PSC area in metastasis is due only to vasogenic edema while in glioblastoma it is attributable to tumor infiltration and/or vasogenic edema. Third, our study did not include other functional MR techniques such as perfusion imaging and MR spectroscopy [25,26]. Comparative studies using these techniques are needed to assess the usefulness of NODDI for differentiating glioblastoma from brain metastasis.

Conclusion

NODDI compartment maps, especially VEC maps, in the PSC area were useful for differentiating glioblastoma from solitary brain metastasis.

Disclosure of interest

The authors declare that they have no competing interest.

Acknowledgment

This work was supported by JSPS KAKENHI Grant Number 17851674.

Références

[1] Louis DN, Ohgaki H, Wiestler OD, Cavenee WK, Ellison DW, Figarella-Branger D, et al. WHO classification of tumours of the central nervous system. Lyon, France: International Agency for Research on Cancer; 2016.
[2] Giese A, Westphal M. Treatment of malignant glioma: a problem beyond the margins of resection. J Cancer Res Clin Oncol 2001;127:217–25.
[3] Soffietti R, Ruda R, Mutani R. Management of brain metastases. J Neurol 2002;249:1357–69.
[4] Schiff D. Single brain metastasis. Curr Treat Options Neurol 2001;3:89–99.
[5] Lu S, Ahn D, Johnson G, Law M, Zagzag D, Grossman RI. Diffusion-tensor MR imaging of intracranial neoplasia and associated peritumoral edema: introduction of the tumor infiltration index. Radiology 2004;232:221–8.
[6] Lu S, Ahn D, Johnson G, Cha S. Peritumoral diffusion tensor imaging of high-grade gliomas and metastatic brain tumors. AJNR Am J Neuroradiol 2003;24:937–41.
[7] Byrnes TJ, Barrick TR, Bell BA, Clark CA. Diffusion tensor imaging discriminates between glioblastoma and cerebral metastases in vivo. NMR Biomed 2011;24:54–60.
[8] Lee EJ, terBrugge K, Mikulis D, Choi DS, Bae JM, Lee SK, et al. Diagnostic value of peritumoral minimum apparent diffusion coefficient for differentiation of glioblastoma multiforme from solitary metastatic lesions. AJR Am J Roentgenol 2011;196:71–6.
[9] Wang S, Kim S, Chawla S, Wolf RL, Zhang WG, O'Rourke DM, et al. Differentiation between glioblastoma and solitary brain metastases using diffusion tensor imaging. Neuroimage 2009;44:653–60.
[10] Toh CH, Wei KC, Ng SH, Wan YL, Lin CP, Castillo M. Differentiation of brain abscesses from necrotic glioblastomas and cystic metastatic brain tumors with diffusion tensor imaging. AJNR Am J Neuroradiol 2011;32:1646–51.
[11] Wang S, Kim SJ, Poptani H, Woo JH, Mohan S, Jin R, et al. Diagnostic utility of diffusion tensor imaging in differentiating glioblastomas from brain metastases. AJNR Am J Neuroradiol 2014;35:928–34.
[12] Calli C, Kitis O, Yunten N, Yurtseven T, Islekel S, Akalin T. Perfusion and diffusion MR imaging in enhancing malignant cerebral tumors. Eur J Radiol 2006;58:394–403.
[13] Tsuchiya K, Fujikawa A, Nakajima M, Honya K. Differentiation between solitary brain metastasis and high-grade glioma by diffusion tensor imaging. Br J Radiol 2005;78:533–7.
[14] Zhang H, Schneider T, Wheeler-Kingshott CA, Alexander DC. NODDI: practical in vivo neurite orientation dispersion and density imaging of the human brain. Neuroimage 2012;61:1000–16.
[15] Winston GP, Micallef C, Symms MR, Alexander DC, Duncan JS, Zhang H. Advanced diffusion imaging sequences could aid assessing patients with focal cortical dysplasia and epilepsy. Epilepsy Res 2014;108:336–9.
[16] Kamagata K, Hatano T, Okuzumi A, Motoi Y, Abe O, Shimoji K, et al. Neurite orientation and density imaging in the substantia nigra in idiopathic Parkinson disease. Eur Radiol 2016;26:2567–77.
[17] Irie R, Tsuruta K, Hori M, Suzuki M, Kamagata K, Nakanishi A, et al. Neurite orientation dispersion and density imaging for evaluation of corticospinal tract in idiopathic normal pressure hydrocephalus. Jpn J Radiol 2017;35:25–30.
[18] Caverzasi E, Papinutto N, Castellano A, Zhu AH, Scifo P, Riva M, et al. Neurite orientation dispersion and density imaging color maps to characterize brain diffusion in neurologic disorders. J Neuroimaging 2016;26:494–8.
[19] Wen Q, Kelley DA, Banerjee S, Lupo JM, Chang SM, Xu D, et al. Clinically feasible NODDI characterization of glioma using multiband EPI at 7T. Neuroimage Clin 2015;9:291–9.
[20] Pekmezci M, Perry A. Neuropathology of brain metastases. Surg Neurol Int 2013;4(Suppl. 4):245–55.
[21] Lunsford LD, Martinez AJ, Latchaw RE. Magnetic resonance imaging does not define tumor boundaries. Acta Radiol Suppl 1986;369:154–6.
[22] Kelly PJ, Daumas-Duport C, Kispert DB, Kall BA, Scheithauer BW, Illig JJ. Imaging-based stereotaxic serial biopsies in untreated intracranial glial neoplasm. J Neurosurg 1987;66:865–74.
[23] Watanabe M, Tanaka R, Takeda N. Magnetic resonance imaging and histopathology of cerebral gliomas. Neuroradiology 1992;34:463–9.
[24] Price SJ, Jena R, Burnet NG, Hutchinson PJ, Dean AF, Pena A, et al. Improved delineation of glioma margins and regions of infiltration with the use of diffusion tensor imaging: an image-guided biopsy study. AJNR Am J Neuroradiol 2006;27:1969–74.
[25] Law M, Cha S, Knopp EA, Johnson G, Arnett J, Litt AW. High-grade gliomas and solitary metastases: differentiation by using perfusion and proton spectroscopic MR imaging. Radiology 2002;222:715–21.
[26] Cha S, Lupo JM, Chen MH, Lamborn KR, McDermott MW, Berger MS, et al. Differentiation of glioblastoma multiforme and single brain metastasis by peak height and percentage of signal intensity recovery derived from dynamic susceptibility-weighted contrast-enhanced perfusion MR imaging. AJNR Am J Neuroradiol 2007;28:1078–84.